Supporting Information for

The effect of CO_2 ramping rate on the transient weakening of the Atlantic Meridional Overturning Circulation

Camille Hankel

Camille Hankel.
E-mail: crhankel@uw.edu

This PDF file includes:

Figs. S1 to S14
SI References

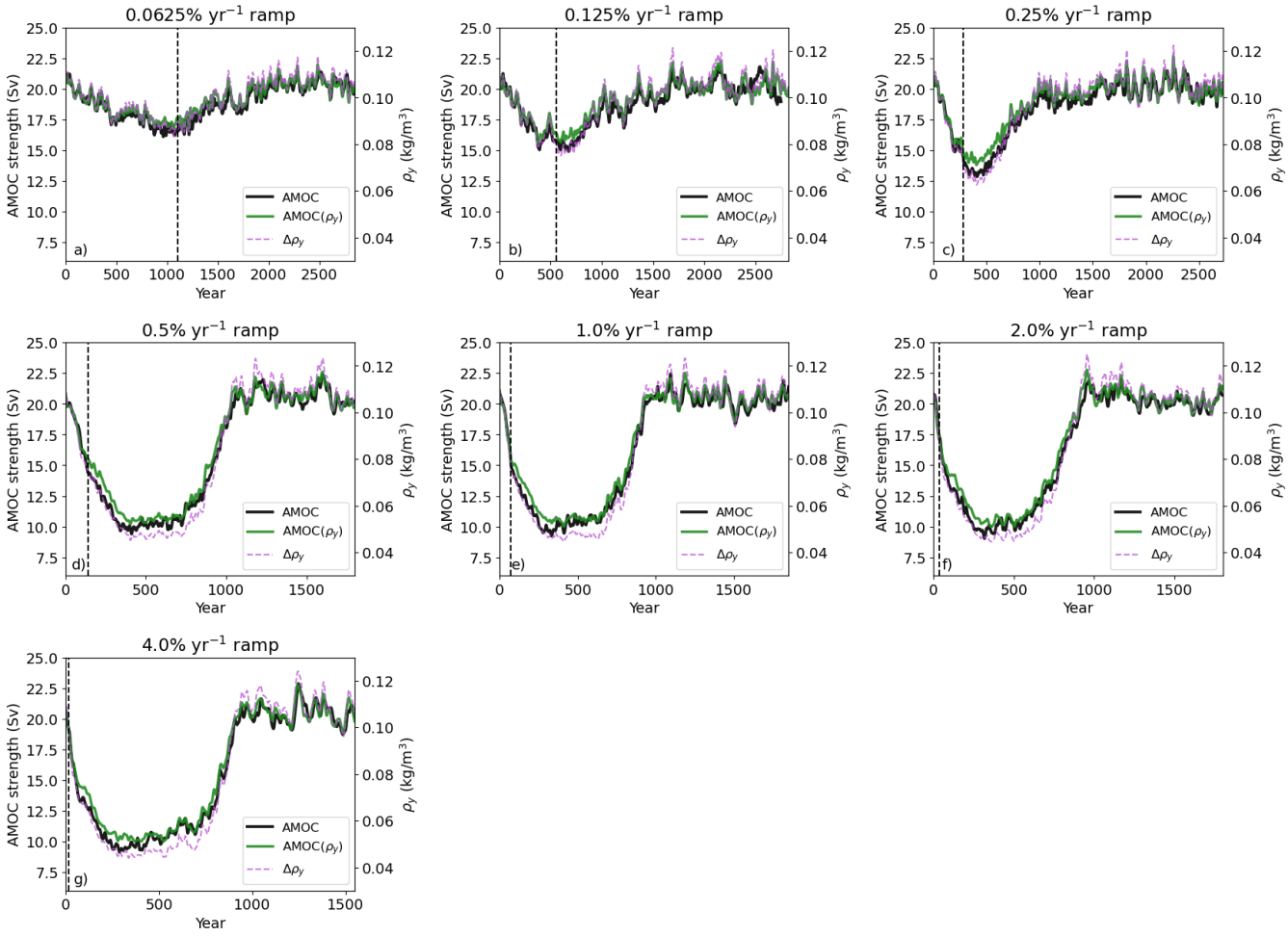

Fig. S1. AMOC strength from the model output overturning streamfunction ('MOC' variable) in black, and calculated from the streamfunction reconstruction using meridional density gradients in green for all of the ramping experiments. The dashed magenta line indicates the bulk upper ocean (vertically averaged over 500 m and 2500 m depth) meridional density gradient between the North and South Alantic regions using the right y-axis. Vertical dashed lines again indicate the year in which 2xCO_2 is reached for each experiment, after which it is held fixed.

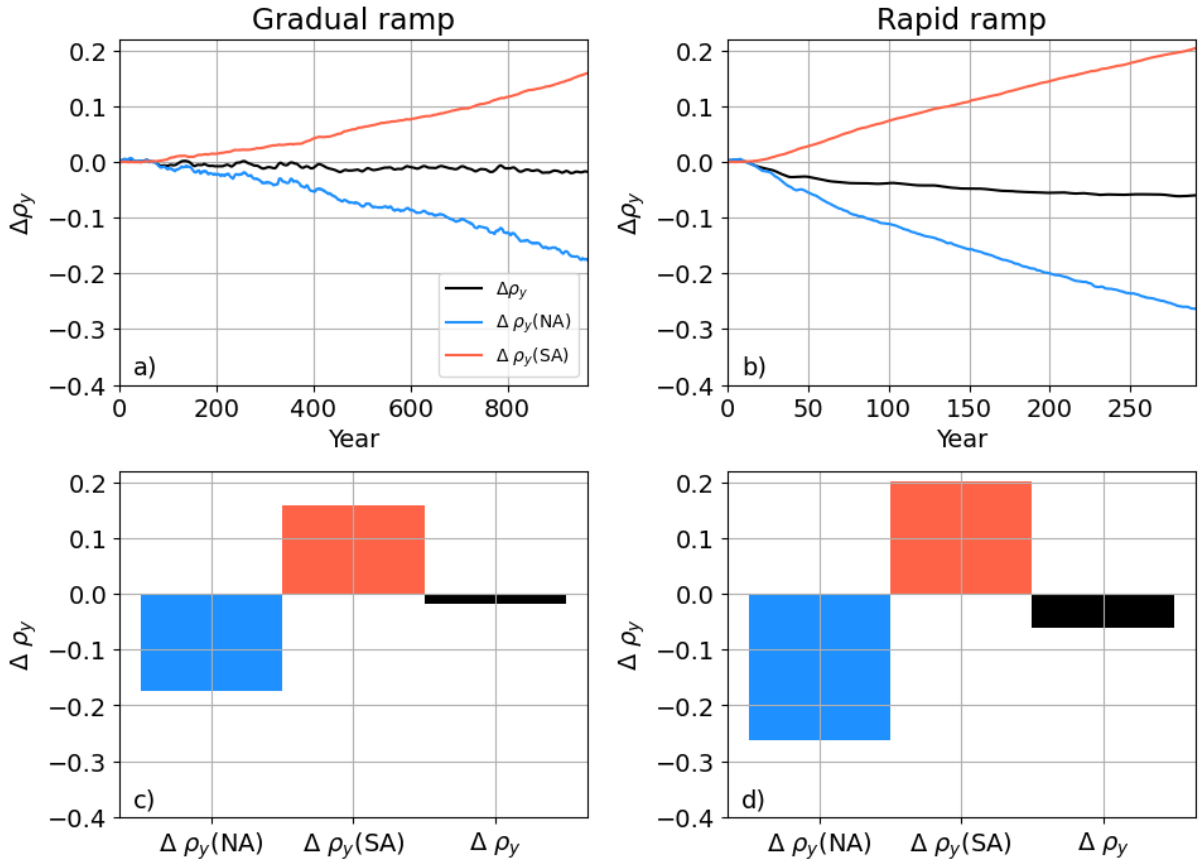

Fig. S2. Contributions of density changes in the North Atlantic (blue lines/bars) and South Atlantic (red) to changes in the bulk meridional density gradient in the two endmember ramping experiments. The "bulk" density/density gradient is defined the same as in Fig. S1. Panels (a) and (b) show these contributions over the period of time leading to the minimum AMOC strength for the most gradual ramping experiment (0.0625% CO_2 increase per year) and the most rapid ramping experiment (4% CO_2 increase per year) respectively. Panels (c) and (d) show the net change of these quantities over the time period considered (calculated as an average over the last five years of the time period minus the average of the first five years of the period). Note that positive values for the South Atlantic indicate that bulk density is decreasing there, leading to an increase in the meridional density gradient.

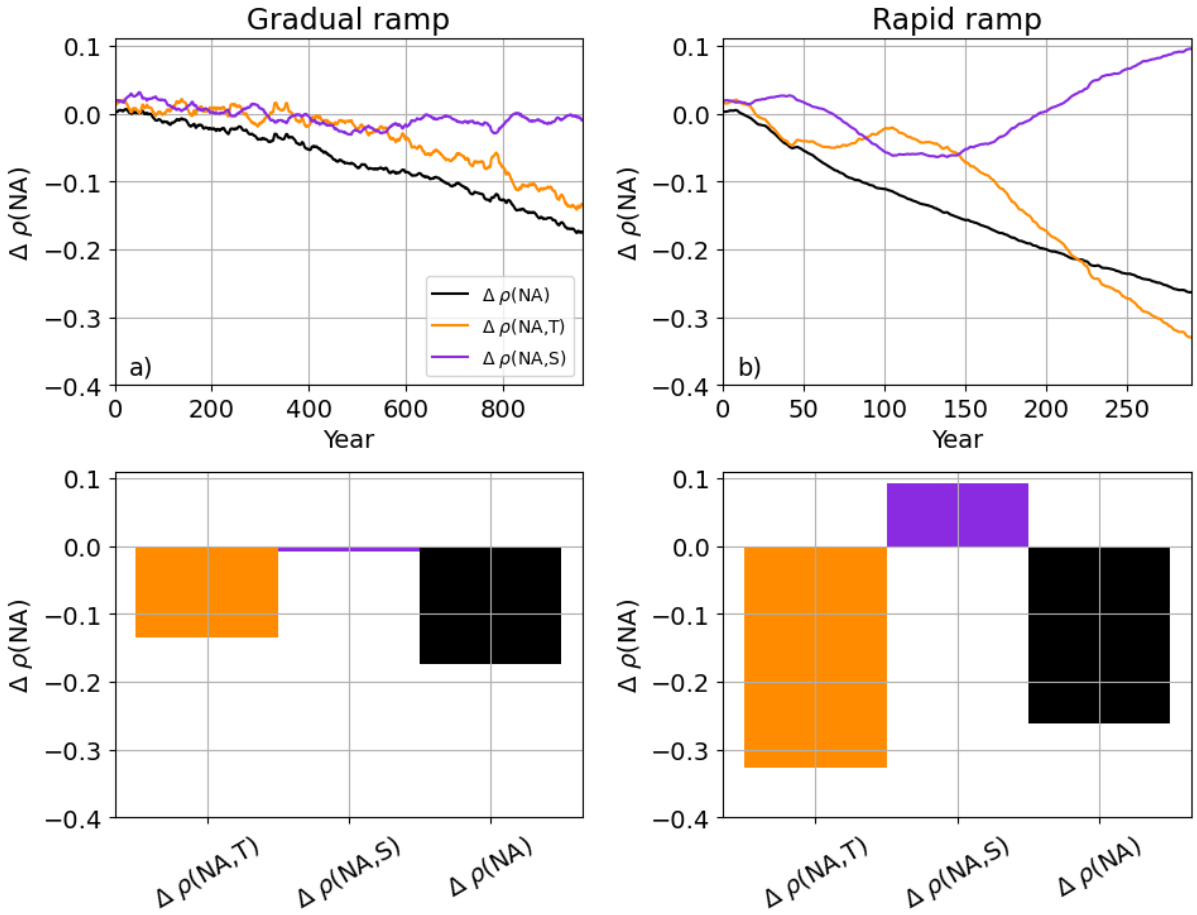

Fig. S3. Bulk upper ocean (same as Fig. S1 and S2) contributions of temperature (orange lines/bar) and salinity (purple) changes to density changes from preindustrial in the North Atlantic region over the period of AMOC weakening for the two end-member experiments. Panels are the same as S2

.

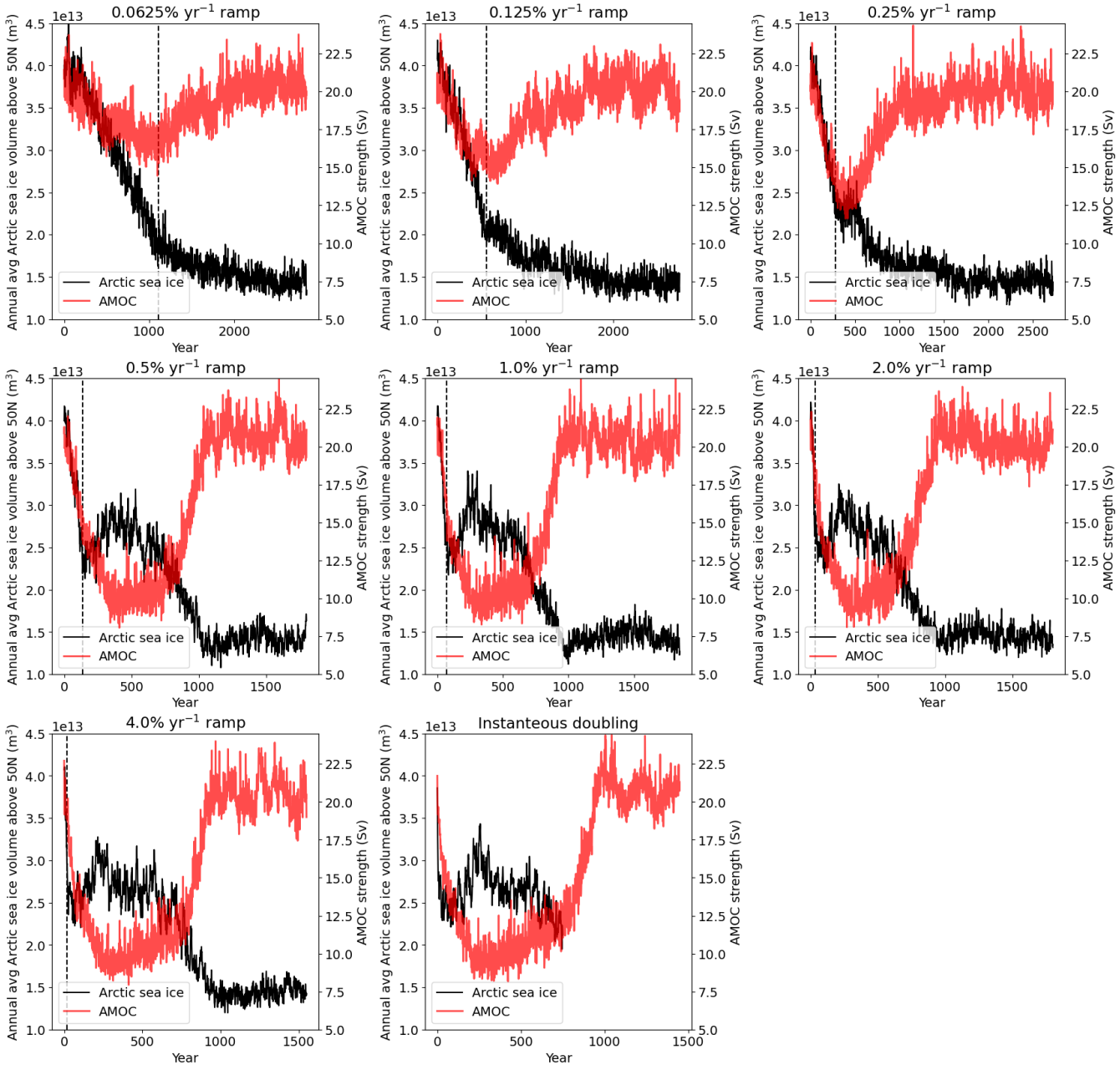

Fig. S4. Annual average total Arctic sea ice volume shown in black (using the left y-axis) and AMOC strength in red (using the right y-axis) across the 7 ramping experiments and the one instantaneous CO_2 doubling experiment (for as long as the sea ice output was saved) as indicated in the panel titles. The vertical dashed line indicates the year in which $2xCO_2$ is reached.

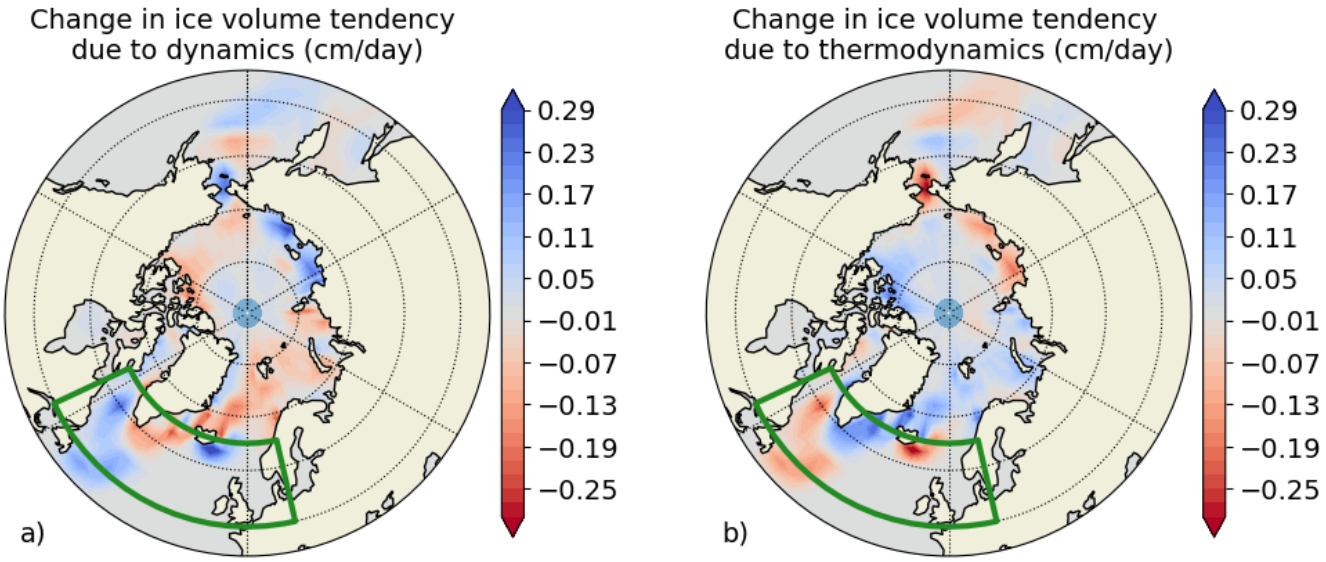

Fig. S5. Absolute change in ice growth tendency over the period of sea ice re-growth (years 67-210) during the most rapid ramping experiment (4% CO_2 increase per year). Panel (a) shows changes in the ice growth tendency due to ice dynamics (import/export of ice) and panel (b) shows changes due to ice thermodynamics (growth/melting of ice). The green box indicates the North Atlantic region over which the surface freshwater fluxes are calculated in Figure 3 of the main text.

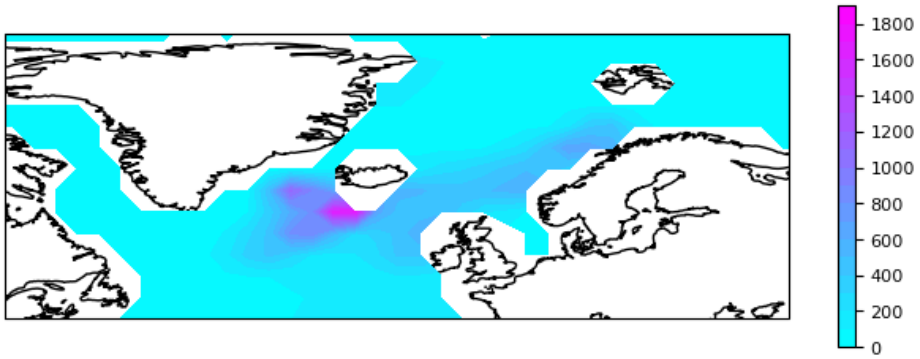

Fig. S6. March maximum ocean mixed layer depth (m) averaged over the last 30 years of the preindustrial spinup run, indicating the regions of deep convection that mark the terminus of the AMOC.

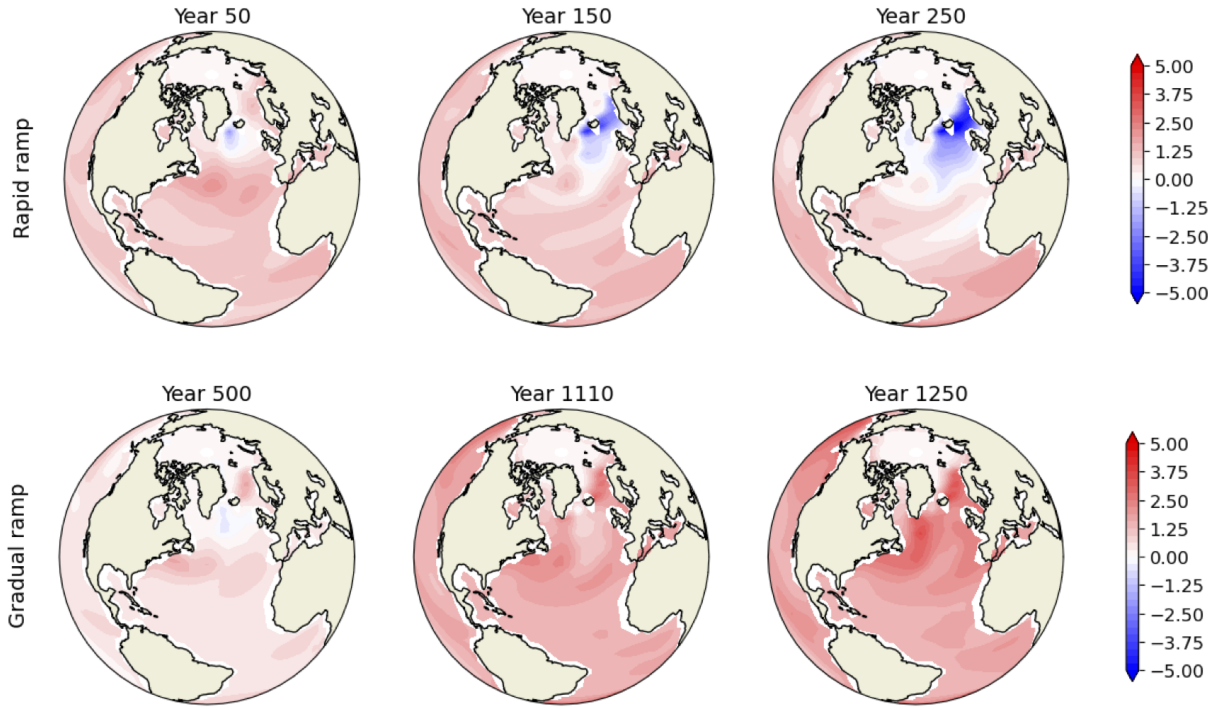

Fig. S7. Sea surface temperature anomalies (K) from preindustrial at three different times of the 4%/year ramping experiment spanning the period of sea ice regrowth and AMOC decline (top row). The bottom row shows the same quantity for three selected periods of the 0.0625%/year ramping experiment (before, at, and after the experiment reaches 2xCO_2), as the AMOC undergoes a more modest decline. The gradual experiment exhibits some evidence of a North Atlantic 'warming hole', but does not show a noticeable SST cooling anomaly like the rapid experiment. Each panel consists of a 10-year average centered around the year indicated in the title.

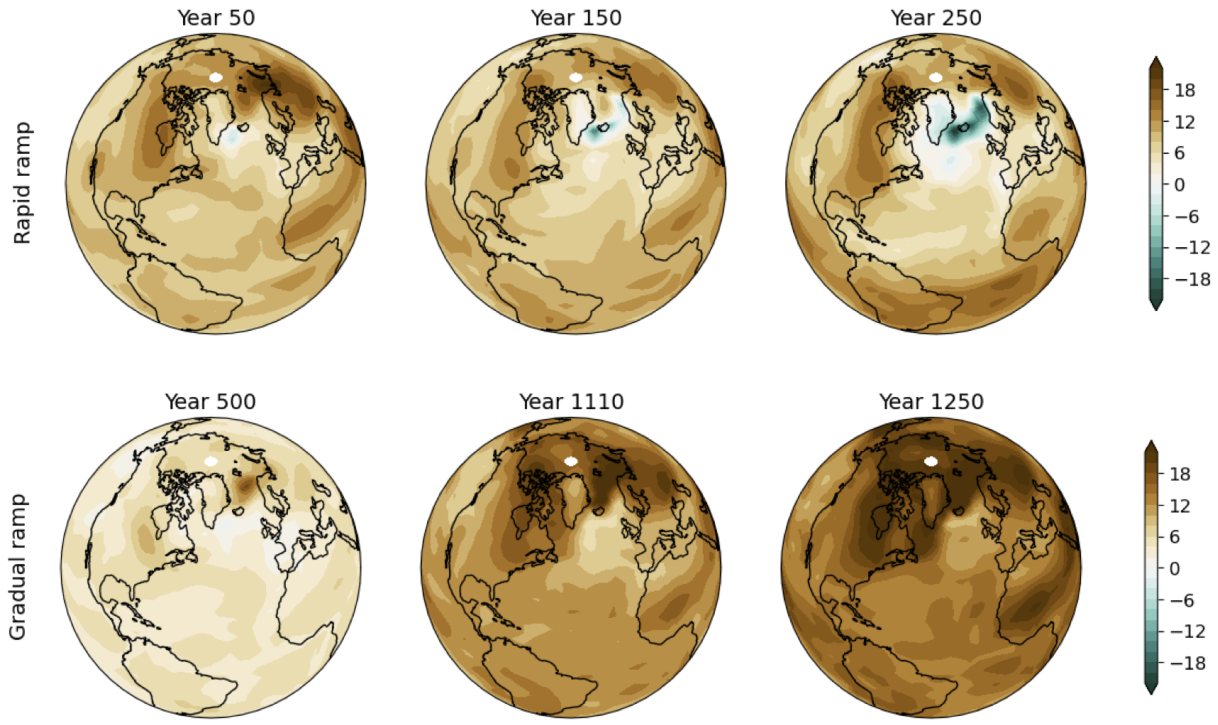

Fig. S8. Changes in longwave downwelling (W/m^2) at the surface from preindustrial as 10-year averages centered around the three years indicated in the title for the 4%/year ramping experiment (top row) and the 0.0625%/year ramping experiment (bottom row).

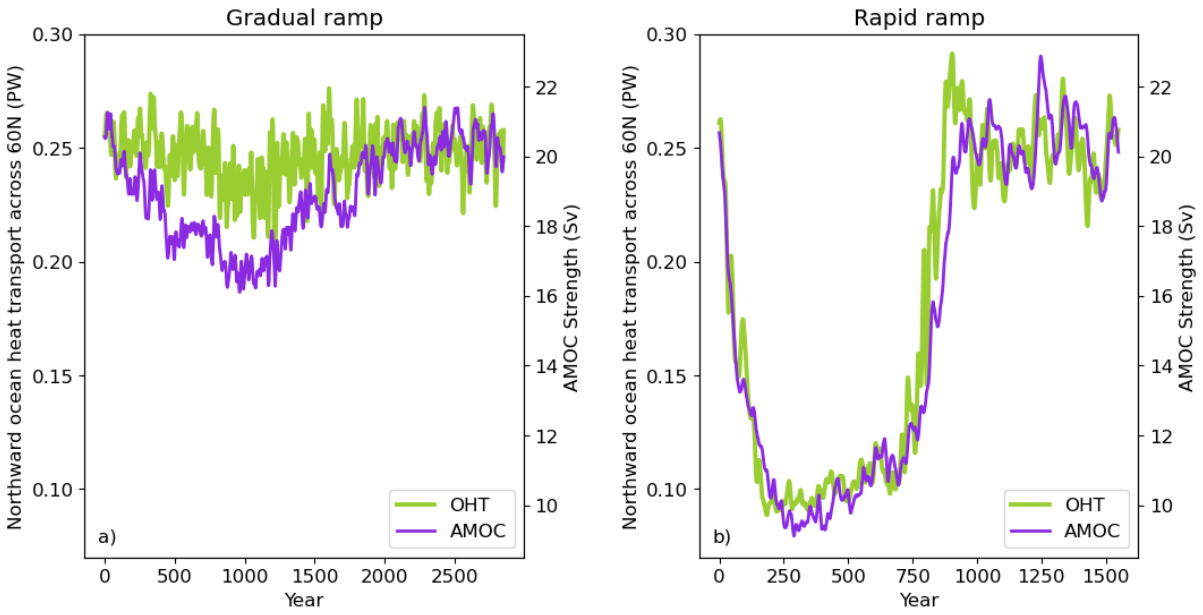

Fig. S9. Northward ocean heat transport across 60°N (left axis, green lines) and the AMOC strength (right axis, purple lines) for the most gradual ramping experiment (a) and the most rapid ramping experiment (b). Ten-year linear smoothing has been applied twice to all timeseries.

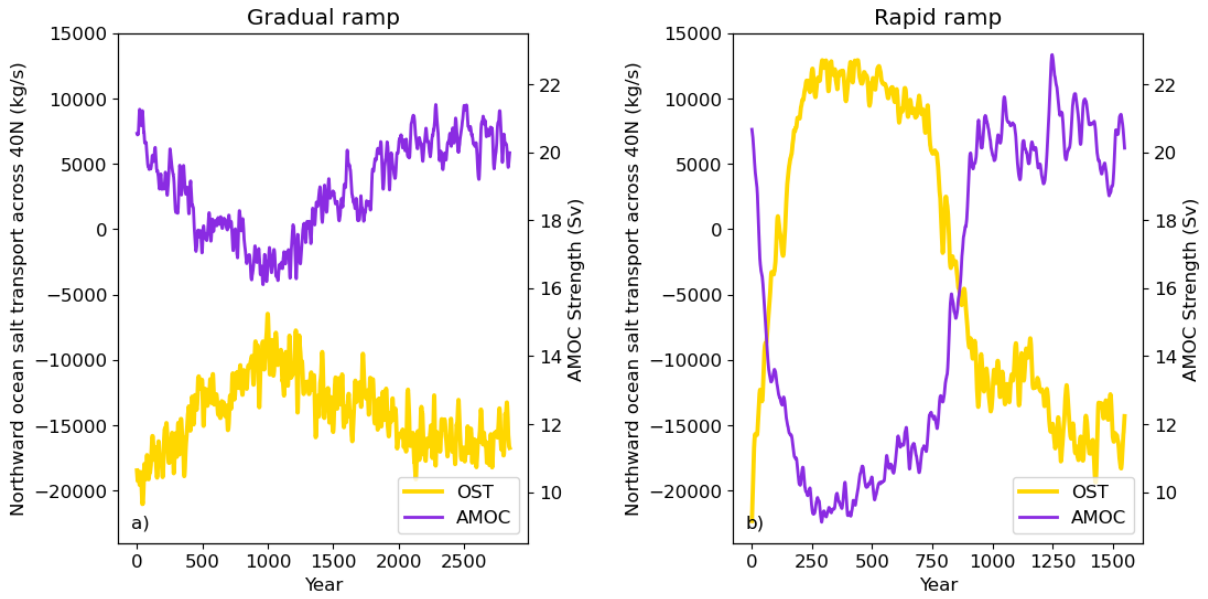

Fig. S10. Net northward ocean salt transport across 40°N in the Atlantic (left axis, yellow lines) and the AMOC strength (right axis, purple lines) for the most gradual ramping experiment (a) and the most rapid ramping experiment (b). The northward salt transport is the sum of all the transport components (including the Eulerian mean, eddy, and submesoscale contributions) of the 'N_SALT' variable in CESM. The model calculates this variable at each latitude as the integral in depth and longitude of ocean salinity multiplied by northward velocity. A negative value of this variable indicates that, in total, more salt is being transported southward by the lower ocean (where the northward velocity is negative) than northward by the upper ocean (where the northward velocity is positive). Ten-year linear smoothing has been applied twice to all timeseries.

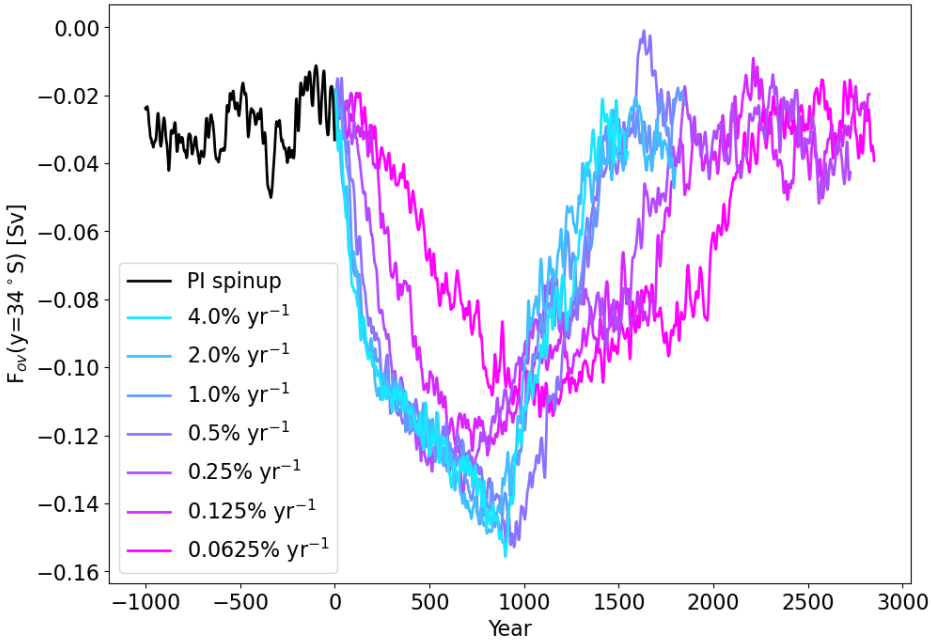

Fig. S11. The net freshwater transport by the overturning circulation (F_{ov}) into the Atlantic basin, calculated following (1), and evaluated at 34°S. By the end of the preindustrial spinup, the net freshwater transport by the circulation is slightly biased positive relative to observational estimates (which range from -.34 Sv to -.05 Sv, 2, 3), but not enough to change its sign. A negative net freshwater transport means that the salt-advective feedback is *positive* in this model configuration (as it is in observations) and that the AMOC could have multiple steady-states for the same CO_2 forcing, although no alternative steady state were discovered under a single doubling of CO_2.

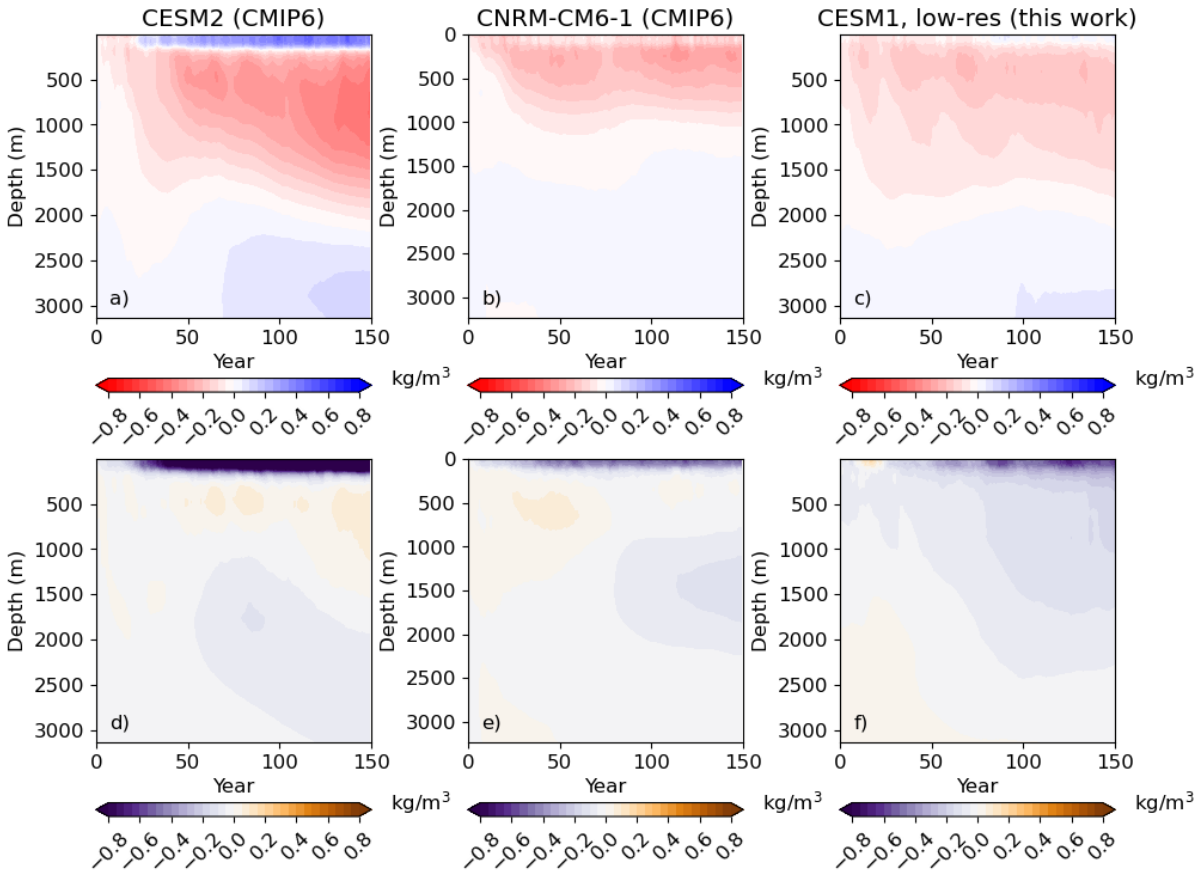

Fig. S12. North Atlantic density changes in two CMIP6 models (with nominal 1-degree horizontal resolution) compared to this work, all run with an instantaneous doubling of atmospheric CO_2. Panels a–c show density changes from preindustrial due to temperature in CESM2, CNRM-CM6-1, and in the low-resolution configuration of CESM1 used here. Panels d–f show density changes from preindustrial due to salinity for the same three models. All models exhibit subsurface warming and surface freshening, suggesting the cross-model importance of the freshwater 'cap' for reducing North Atlantic densities and weakening the AMOC. While CESM2 seems to exhibit a much larger signal (of both warming and freshening), CESM1 develops the same magnitude signal in the next century (similar to what is seen in main text Figures 3b and 3d). It is, therefore, possible that the difference between CESM1 and CESM2 lies in the timing, rather than in the magnitude of the ocean's response to CO_2 doubling.

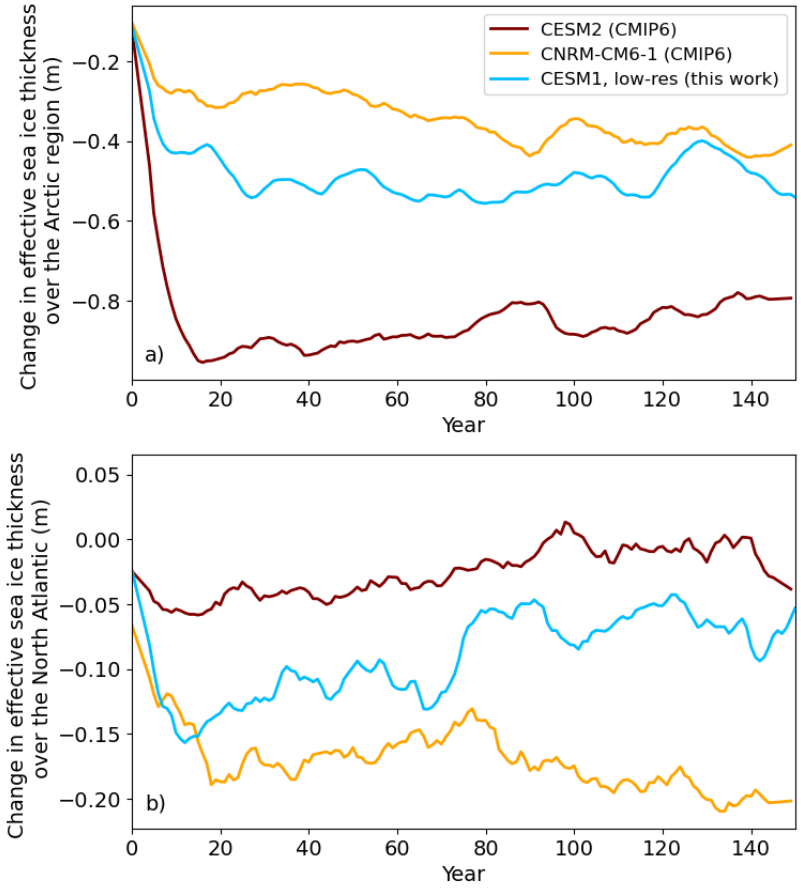

Fig. S13. Arctic sea ice changes in two CMIP6 models and in this work after an instantaneous doubling of atmospheric CO_2. Panel a shows the change in effective sea ice thickness from preindustrial (sea ice volume divided by area of the ocean) for the entire Arctic, considered to be the region above 50°N. Panel b shows the change in effective ice thickness for the portion of the Arctic that lies in the North Atlantic box (50°N–65°N). The CMIP6 models both exhibit a period of sea ice re-growth in the North Atlantic region (even if it is less evident in the Arctic-wide average), which may contribute to the surface freshening seen in Figure S12 as it does in CESM1. The CMIP6 models did not report all the surface freshwater flux components needed to confirm the relative contributions of sea ice melt, net precipitation, and other fluxes to North Atlantic surface freshening.

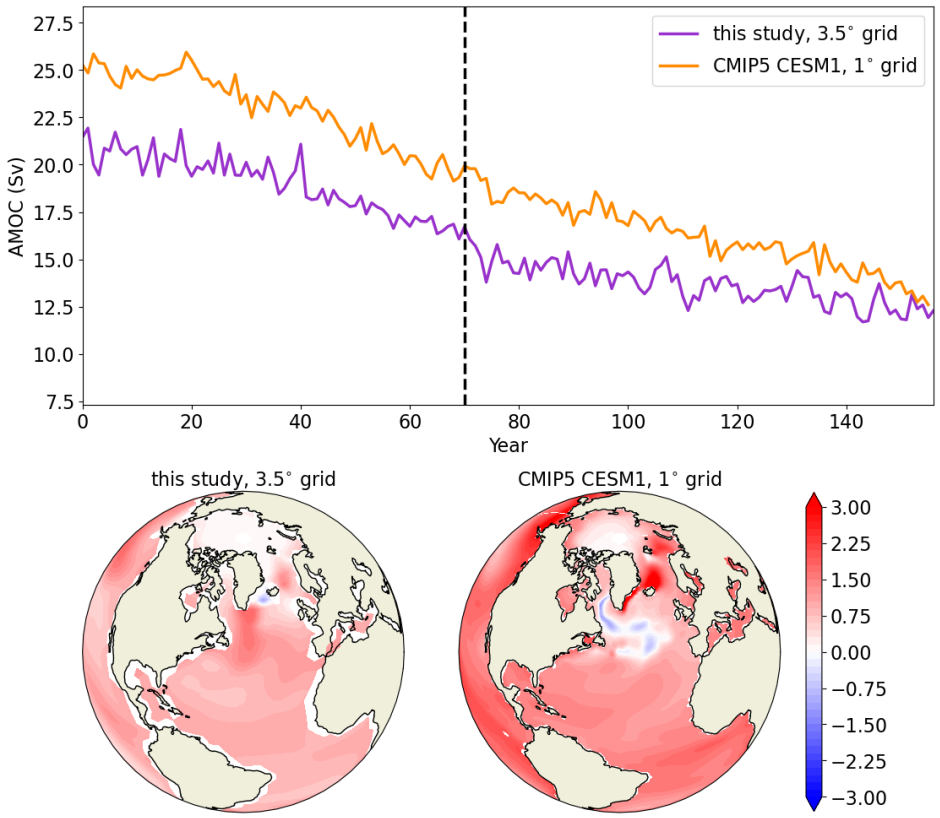

Fig. S14. Comparison of this work to a higher resolution ($\approx 1°$ in the horizontal) version of CESM1 run in CMIP5. The upper panel shows the decline in AMOC strength for the first 150 years of the 1%/year CO_2 ramping experiment conducted in this study, and the 1%/year CO_2 increase experiment run for CESM1 as part of CMIP5. Note that after the experiments reach 2xCO_2 (indicated by the vertical dashed line) they should no longer be compared directly, as the CMIP5 experiment continues to increase CO_2 concentrations at 1%/year while in this study the concentrations are held fixed. Below, the contour maps show the change in sea surface temperature from preindustrial in the two experiments as an average over years 60–70, the last decade before 2xCO_2 is reached. While the magnitude of the sea surface cooling signals for the two models are comparable, their spatial extents differ. This can likely be explained by the spatial extent of the deep convection zone in the higher resolution model, which takes on a more spatially diffuse area that closely mirrors the shape of the cooling signal, while the coarse resolution model has a narrow deep convection zone concentrated off the coast of Iceland, shown in Figure S6.

References

1. RM van Westen, HA Dijkstra, Asymmetry of amoc hysteresis in a state-of-the-art global climate model. *Geophys. Res. Lett.* **50**, e2023GL106088 (2023).
2. SL Garzoli, MO Baringer, S Dong, RC Perez, Q Yao, South atlantic meridional fluxes. *Deep. Sea Res. Part I: Oceanogr. Res. Pap.* **71**, 21–32 (2013).
3. HL Bryden, BA King, GD McCarthy, South atlantic overturning circulation at 24 s. *J. Mar. Res.* (2011).